frontiers in Earth Science

ORIGINAL RESEARCH
published: 22 March 2022
doi: 10.3389/feart.2022.844605

Geochemical and Isotopic Characteristics of Two Geothermal Systems at the Nanpu Sag, Northern Bohai Bay Basin

Ke Wang[1,2,3], Cong Hua[4], Lu Ren[5], Yanlong Kong[1,2,3], Wenjie Sun[6]*, Sheng Pan[7], Yuanzhi Cheng[1,2,3], Yonghui Huang[1,2,3], Fei Tian[1,2,3], Weizun Zhang[1,6], Dajun Qin[1,2,3], Feng Ma[8,9], Jianwei Wang[5] and Yuexia Dong[10]*

[1]Key Laboratory of Shale Gas and Geoengineering, Institute of Geology and Geophysics, Chinese Academy of Sciences, Beijing, China, [2]Innovation Academy for Earth Science, Chinese Academy of Sciences, Beijing, China, [3]College of Earth and Planetary Sciences, University of Chinese Academy of Sciences, Beijing, China, [4]Key Laboratory of Groundwater Resources and Environment, Ministry of Education, College of Environment and Resources, Jilin University, Changchun, China, [5]Jidong Oilfield Company of PetroChina, Tangshan, China, [6]College of Geoscience and Surveying Engineering, China University of Mining and Technology (Beijing), Beijing, China, [7]Key Laboratory of Continental Collision and Plateau Uplift, Institute of Tibetan Plateau Research, Chinese Academy of Sciences, Beijing, China, [8]The Institute of Hydrogeology and Environmental Geology, Chinese Academy of Geological Sciences, Shijiazhuang, China, [9]Technology Innovation Center for Geothermal and Hot Dry Rock Exploration and Development, Ministry of Natural Resources, Shijiazhuang, China, [10]Advisory Center, China National Petroleum Corporation, Shijiazhuang, China

OPEN ACCESS

Edited by:
Ryan Mathur,
Juniata College, United States

Reviewed by:
Ying Li,
China Earthquake Administration, China
Aisha Al Suwaidi,
Khalifa University, United Arab Emirates

***Correspondence:**
Yanlong Kong
ylkong@mail.iggcas.ac.cn
Wenjie Sun
swj@cumtb.edu.cn

Specialty section:
This article was submitted to Economic Geology, a section of the journal Frontiers in Earth Science

Received: *28 December 2021*
Accepted: *23 February 2022*
Published: *22 March 2022*

Citation:
Wang K, Hua C, Ren L, Kong Y, Sun W, Pan S, Cheng Y, Huang Y, Tian F, Zhang W, Qin D, Ma F, Wang J and Dong Y (2022) Geochemical and Isotopic Characteristics of Two Geothermal Systems at the Nanpu Sag, Northern Bohai Bay Basin. Front. Earth Sci. 10:844605. doi: 10.3389/feart.2022.844605

The utilization of geothermal energy has gradually increased in northern China because of its unique advantages as a heating supply. However, the sustainable exploitation of geothermal energy usually requires a comprehensive investigation of the geothermal water circulation pattern prevailing at a proposed site. During the exploitation of geothermal energy resources at Nanpu Sag in northern China, thermal anomalies were found to exist in two adjacent regions: the Caofeidian and the Matouying. To reconcile the anomalies and to examine both the source of recharge water and the geothermal systems' circulation dynamics, a comprehensive investigation was performed using multiple chemical and isotopic tracers (δ^2H, δ^{18}O, ^{87}Sr/^{86}Sr, δ^{13}C, and ^{14}C). The total dissolved solids (TDS) of the geothermal water are approximately 750 mg/L and 1,250 mg/L, respectively. The geothermal water isotopes at the two sites are also different, with average values of -9.3‰ and -8.2‰ for δ^{18}O and -73.4‰ and -71‰ for δ^2H, respectively. Moreover, the ^{87}Sr/^{86}Sr ratio of geothermal water at Matouying is 0.7185, which is much greater than that of Caofeidian, with an average value of 0.7088. All the results confirm the difference between the two geothermal systems and may explain the two circulation patterns of deep groundwater at Caofeidian and Matouying. The reservoir temperature obtained from theoretical chemical geothermometers is estimated to be 83–92°C at the Caofeidian and 107–137°C at the Matouying, respectively. The corrected ^{14}C age implies a low circulation rate that would allow sufficient time to heat the water at Caofeidian. In addition, we propose a geothermal conceptual model in our study area. This model could provide key information regarding the geothermal sustainable exploitation and the effective management of geothermal resources.

Keywords: hydrothermal energy, geochemical characteristic, isotopic characteristic, two geothermal systems, conceptual model, nanpu sag

INTRODUCTION

Hydrothermal energy is obtained by utilizing the heat or energy from the groundwater within the geothermal systems (Byrappa & Yoshimura, 2012). It is recognized that hydrothermal energy is clean, environmentally friendly, stable, and reliable when people use the heat or energy from hydrothermal water (Rybach, 2003; Marrasso et al., 2018). Besides, hydrothermal energy demonstrates the characteristic of large reservoirs and wide distribution (Wang, 2015a; Shortall et al., 2015; Moya et al., 2018; Lund & Toth, 2021). In northern China, hydrothermal energy is widely used because of its unique advantages as a heating supply (Wang, 2009; Duan et al., 2011; Kong et al., 2014; An et al., 2016; Wang et al., 2018). However, to realize the rational exploitation and utilization of hydrothermal geothermal resources, it is necessary to consider the sustainability of long-term exploitation as well as the environmental and geological consequences of exploitation (Hahnlein, Bayer, Ferguson, & Blum, 2013). To determine the exploitation potential of a hydrothermal system, it is imperative to document the water and heat sources, the thermal reservoir, the water transporting channels, and the thermal caprock of the geothermal field (Pang et al., 2018; Huang et al., 2021a). Although one can easily monitor the temperature and thermal reservoir characteristics of hydrothermal systems, it is difficult to determine the water sources, water flow paths, and heat sources for complicated geochemical processes. Precipitation generally recharges into hydrothermal reservoirs through deep, subsurface circulations. Within the circulation period, the geothermal water is heated from the comparative hot surrounding rocks with which it interacts (Lister, 1980; Le Gal et al., 2018). Therefore, the geochemical characteristics and isotopic composition of geothermal water will change accordingly (Yang et al., 2017). Thus, the combination of geochemical and isotopic characteristics in hydrothermal systems is of great value for determining the origin of the hydrothermal water and characterizing the water-rock-gas interaction process.

In northern China, a typical hydrothermal system known as the Caofeidian has been developed and utilized for many years as a heating supply (Chang et al., 2016; Dong et al., 2021; Wang et al., 2021). However, temperature anomalies have been detected in the geothermal development process at the Matouying, located less than 20 km east of the Caofeidian. The temperature of the geothermal boreholes at the Matouying was found to be much higher than those of the Caofeidian. To distinguish the temperature anomalies and realize the sustainable utilization of hydrothermal energy, it is necessary to investigate the patterns of deep groundwater circulation and geothermal reservoir conditions. Although some geophysical studies have been conducted to investigate the causes of the temperature anomalies within this area, no research has been conducted to compare the hydrothermal waters at the Caofeidian and the Matouying from the geochemical and isotopic information.

In this study, we conducted detailed geochemical and isotopic analyses of geothermal waters at the Caofeidian and the Matouying to distinguish the differences between the two sites and investigate the hydrothermal system characteristics. ^{14}C dating was used to assess the age of deep geothermal groundwater. We also determined the heat source and circulation patterns of different geothermal waters based on their geochemical and isotopic characteristics. The principal research objectives of this study are: 1) to investigate the geochemical and isotopic characteristics of the geothermal groundwater at the Caofeidian and the Matouying; 2) to determine the causes of geothermal water differences between the two areas; and 3) to propose a conceptual model of geothermal water circulation in the research areas.

GEOLOGICAL AND HYDROGEOLOGICAL SETTINGS

Caofeidian is located 80 km south of Tangshan and 120 km east of Tianjin in the north-central part of the Bohai Bay Basin which locates in the northern China (**Figure 1A** and **Figure 2**). In terms of geological structure, the Caofeidian is located in the north of the Nanpu Sag, one of the major oil and gas fields in China (**Figure 2**). The Nanpu depression is located in the north of the Huanghua Depression, and its northwest boundary is the Xinanzhuang fault, separated from the Xinanzhuang Uplift and Laowangzhuang Uplift (**Figure 2**) (Dong et al., 2021). The northeast boundary is the Baigezhuang fault, which is adjacent to the Baigezhuang Uplift and the Matouying Uplift (**Figure 2**). The southern Nanpu depression is in a fault-superposition relationship with the Shaleitian Uplift. Geothermal anomaly zones were found in the Matouying Uplift area near the Baigezhuang fault. The Caofeidian and Matouying areas are located on the west and east sides of the Baigezhuang fault, respectively (**Figure 2**).

In general, Nanpu Sag is a Tertiary sedimentary lake basin (Wang et al., 2022). From the surface downwards, the Nanpu Sag and its surrounding areas are characterized by Cenozoic, Mesozoic, Paleozoic, Neoproterozoic, and Archean strata (Zhu et al., 2014; Wang et al., 2020). The stratigraphic distribution and thickness of different structural units of the Nanpu Sag vary greatly (Wang et al., 2021). Baigezhuang Fault is a border fracture separating Matouying and Nanpu, which has controlling effect on the formation and evolution of Nanpu Sag. Because of the movement of Baigezhaung Fault, the Archean granite was uplifted at Matouying. Besides, the destruction of the eastern North China Craton and the thinning of the regional lithosphere also contributed to the shallow depth of granite at Matouying (Qiu et al., 2014; Qiu et al., 2016; Zhang et al., 2020b; Dong et al., 2021). According to the geophysical work by Dong et al. (2008), the depth of Baigezhuang Fault was estimated to be more than 5 km downwards, which reached the basement of Archean granite. The main heat reservoirs in the Nanpu Sag are the Neogene Guantao Formation and the Neogene Minghuazhen

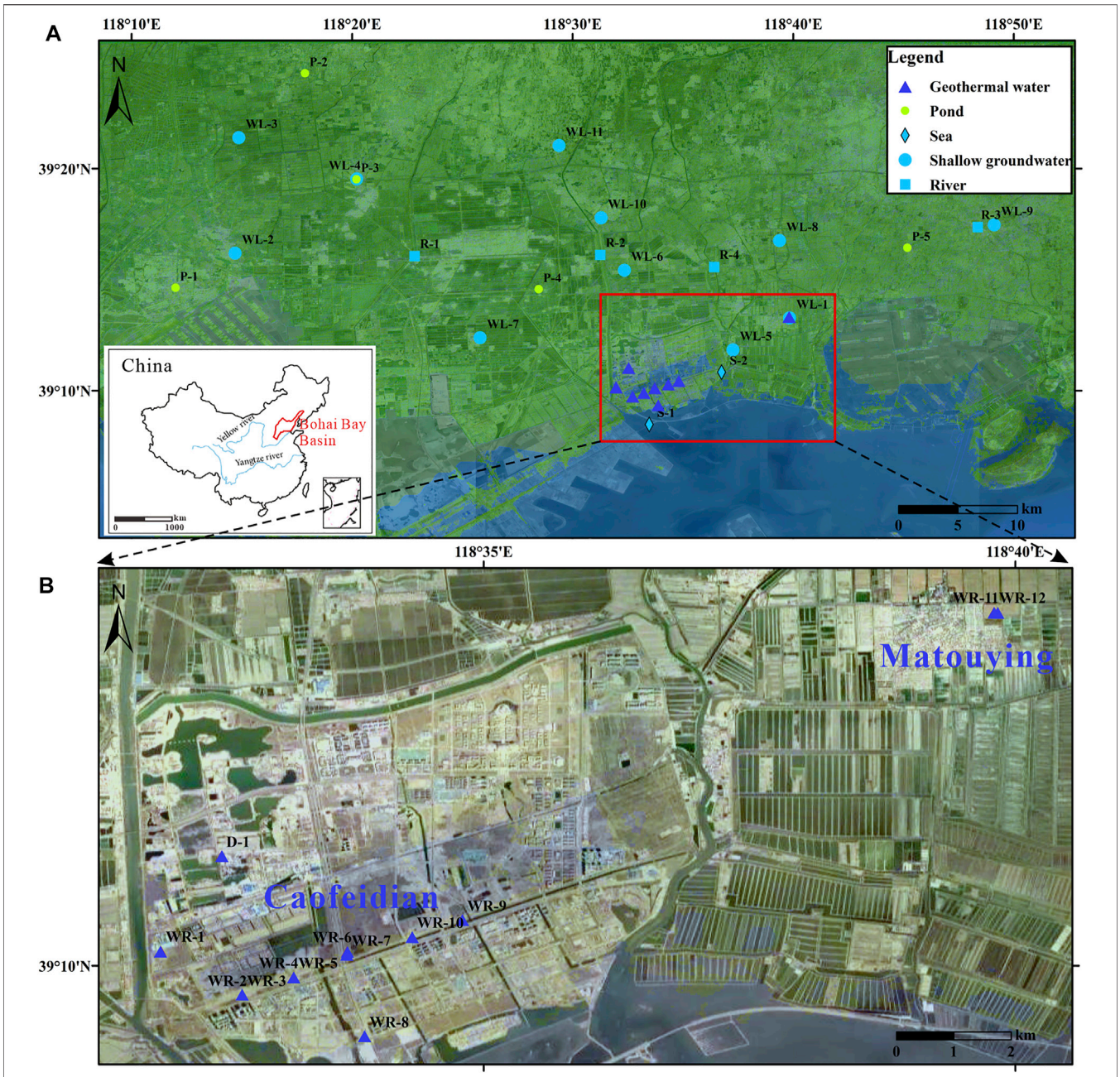

FIGURE 1 | (A): Location of Bohai Bay Basin in China and all the sampling sites in the study area, the red rectangle represents the area where the geothermal water were sampled; **(B)**: The sampling locations of geothermal water in the two regions Caofeidian and Matouying.

Formation (**Figure 3**), followed by the Cambrian and the Ordovician. The Neogene strata is principally driven by the uplift and sag of the Paleogene. Except for the absence of the Laowangzhuang uplift, the Guantao Formation contains a thickness of 300–900 m in our study area except for the Laowangzhuang Uplift. The thermal reservoirs of the Guantao Formation are mainly fine sandstone and gravel sandstone with an average porosity of 30–35%. The bottom boundary of the Guantao Formation thermal reservoir is 2,100–2,600 m deep, gradually increasing in depth from north to south. The Minghuazhen Formation has a thickness of 1,000–2000 m throughout the study region. The bottom boundary of the Minghuazhen Formation's thermal reservoir is 1700–2,200 m deep, gradually deepening from north to south. The Quaternary in this region belongs to the Pleistocene-Holocene strata, which are not integrated with the underlying Minghuazhen Formation. Quaternary in this area is a set of undiagenetic interbedded yellow glutenite and clay,

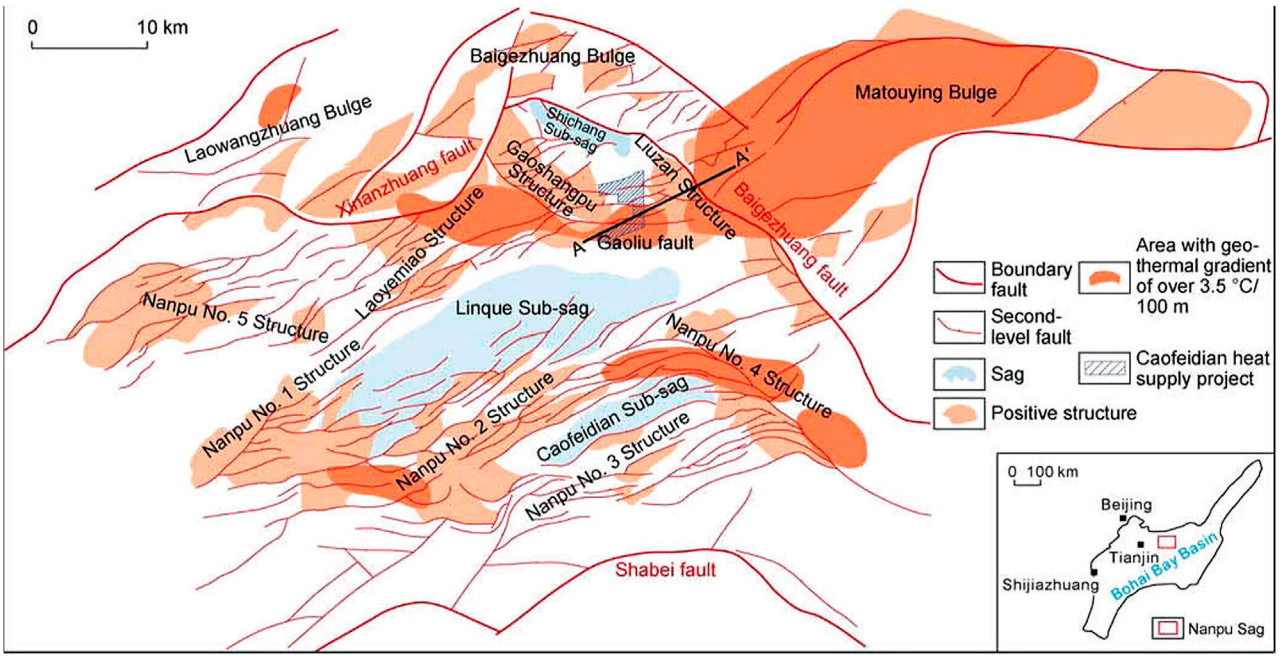

FIGURE 2 | Geological map of the Nanpu Sag and its locations in Bohai Bay Basin (cited from Dong et al., 2021).

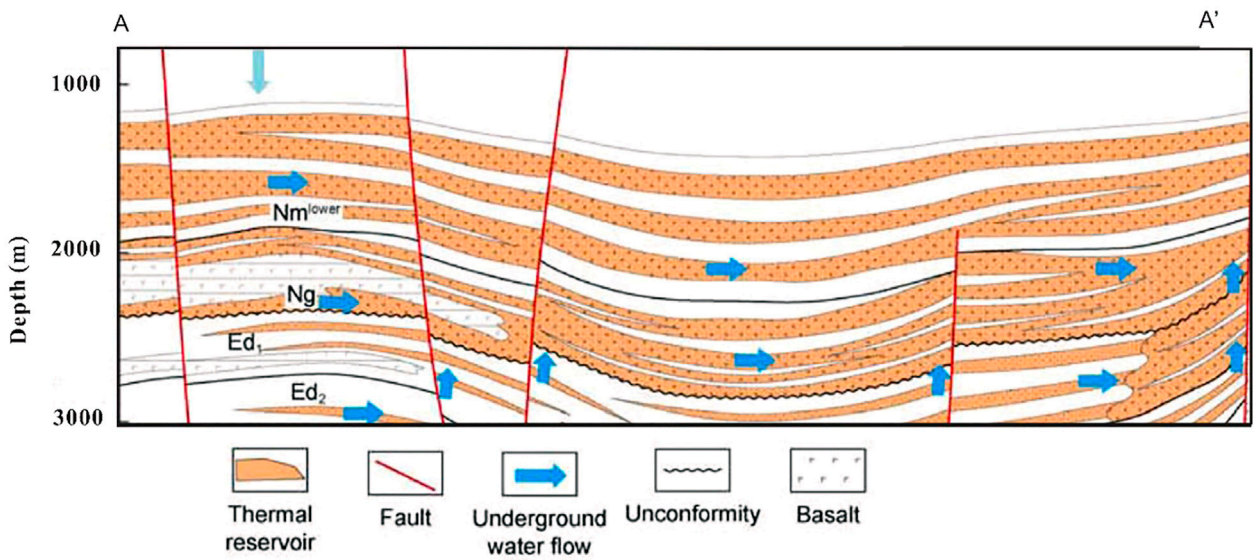

FIGURE 3 | Cross section **(A,A')** of the Nanpu Sag (cited from Huang et al., 2021b).

the bottom of which are alluvial and alluvial glutenite layers. In this study, we focus on the Neogene sandstone aquifer because it is the principal geological formation exploited for geothermal energy production in the Caofeidian and the Matouying. Our study objective is the Neogene heat reservoir. The Neogene strata in the Caofeidian, and the Matouying is mainly porous sandstone, which has the characteristics of high porosity and permeability.

SAMPLING AND ANALYSIS

Field sampling was performed at the Nanpu Sag in December and November 2019. A total of 35 water samples were collected, including 12 from geothermal wells, 11 from shallow wells, and one from deep wells in the Dongying Formation. To compare the hydrochemistry and isotopic characteristics of groundwater and surface water, we also collected four river samples, five pond

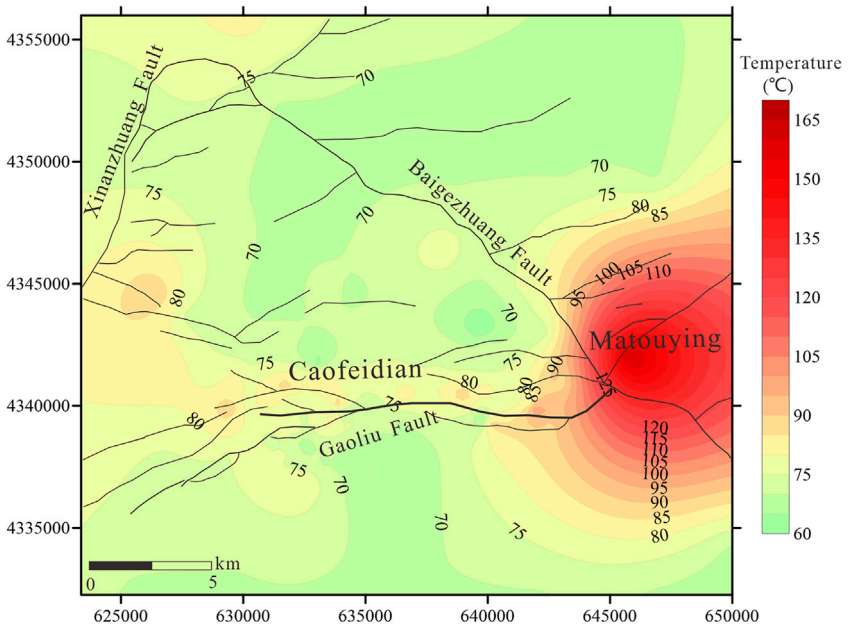

FIGURE 4 | Temperature gradient of the geothermal wells at the depth of 2120m in the study area.

samples, and 2 seawater sample in different directions of the geothermal wells. All sampling locations are shown in **Figure 1A**. The sampling time was within the heat supply period, consequently, the water samples from the geothermal boreholes are representative of the water within the aquifer. All the samples were filtered *in situ* with a 0.23 μm membrane prior to bottling and sealing with Parafilm. Samples for cation and trace element analysis were acidified with ultra-purified HNO_3 to adjust the pH of each sample to less than 2. The acidified process was not added to the samples for anion and water isotope analyses.

Temperature, pH, electrical conductivity (EC), and total dissolved solids (TDS) were measured in the field using a multi-parameter device (Hach HQ40D). HCO_3^- and CO_3^{2-} were measured in the field using a digital titrator (16,900 Digital Titrator, Hach) with indicators including phenolphthalein and methyl orange colorants. The samples were sent for analysis at the Water Isotopes and Water–Rock Interaction Laboratory, Institute of Geology and Geophysics, Chinese Academy of Sciences.

Cations and anions were identified according to the National Analysis standard DZ/T0064.28–93 and DZ/T0064.51–93, respectively. The detection limit was 0.1 mg/L. The trace elements were determined using ICP-MS (7500C, Agilent) with an analytical precision of less than 0.5%. Stable isotopes (δ^2H and $\delta^{18}O$) were measured using a laser absorption water isotope spectrometer analyzer (Picarro L2120-i). All δ^2H and $\delta^{18}O$ values are expressed in δ notation per mil relative to the Vienna Standard Mean Ocean Water (V-SMOW). The measurement precisions of δ^2H and $\delta^{18}O$ were ±0.5‰ and ±0.1‰, respectively. The trace elements were determined using ICP-MS (7500C, Agilent) at the Analytical Laboratory of Beijing Research Institute of Uranium Geology with an analytical precision of less than 0.5%. The carbon isotopic compositions (i.e., ^{14}C and ^{13}C) were determined by Beta Analytic, Inc. using accelerator mass spectrometry (AMS) and isotope ratio mass spectrometry (IR-MS), respectively. The analytical precision of the AMS ^{14}C results was ±0.1%. The ^{14}C ages were corrected using the $\delta^{13}C$ mixing model (Clark and Fritz, 2013):

$$t = -8267\ln\left(\frac{C_t}{qC_0}\right) \quad (1)$$

$$q = \frac{\delta^{13}C_t - \delta^{13}C_d}{\delta^{13}C_s - \delta^{13}C_d} \quad (2)$$

where t is the groundwater age, C_t is the measured ^{14}C activity, q is the correction factor, and $\delta^{13}C_t$, $\delta^{13}C_d$, and $\delta^{13}C_s$ represent the measured $\delta^{13}C$ values for the groundwater, the dissolved calcite (0‰), and soil (-23‰), respectively.

RESULTS

Local Hydrothermal Pattern

The temperature gradient of the geothermal wells is shown in **Figure 4**. By comparing the geothermal water temperature at the Caofeidian and the Matouying, we found significant differences between the two locations. The temperature of the geothermal water sampled at the Matouying has a maximum of 117°C, which is much greater than that of the Caofeidian, 70–80°C. In addition, the geothermal gradient for the Neogene Guantao Formation at Matouying is also much greater than that observed at the Caofeidian, which is about 4.0–7.0 and 2.3–3.9°C/100 m, respectively. Although the distance between the two geothermal

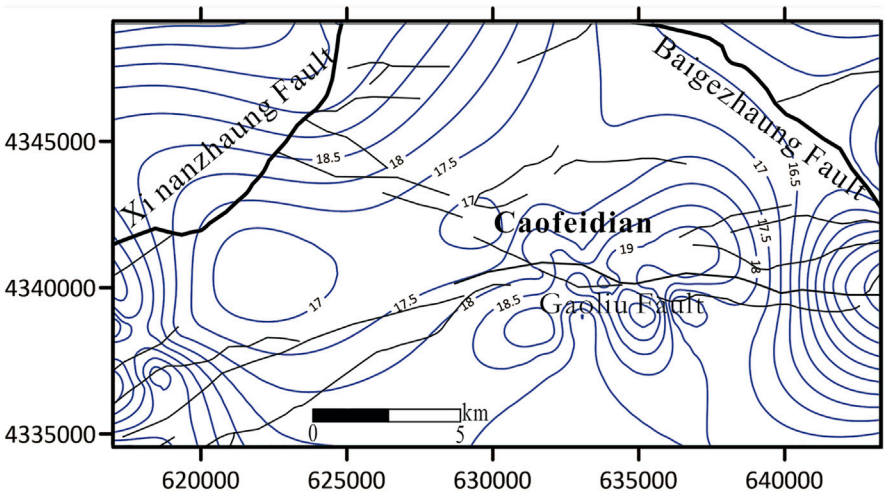

FIGURE 5 | Contours of hydrostatic pressure of the geothermal wells at the depth of 2000m at Caofeidian.

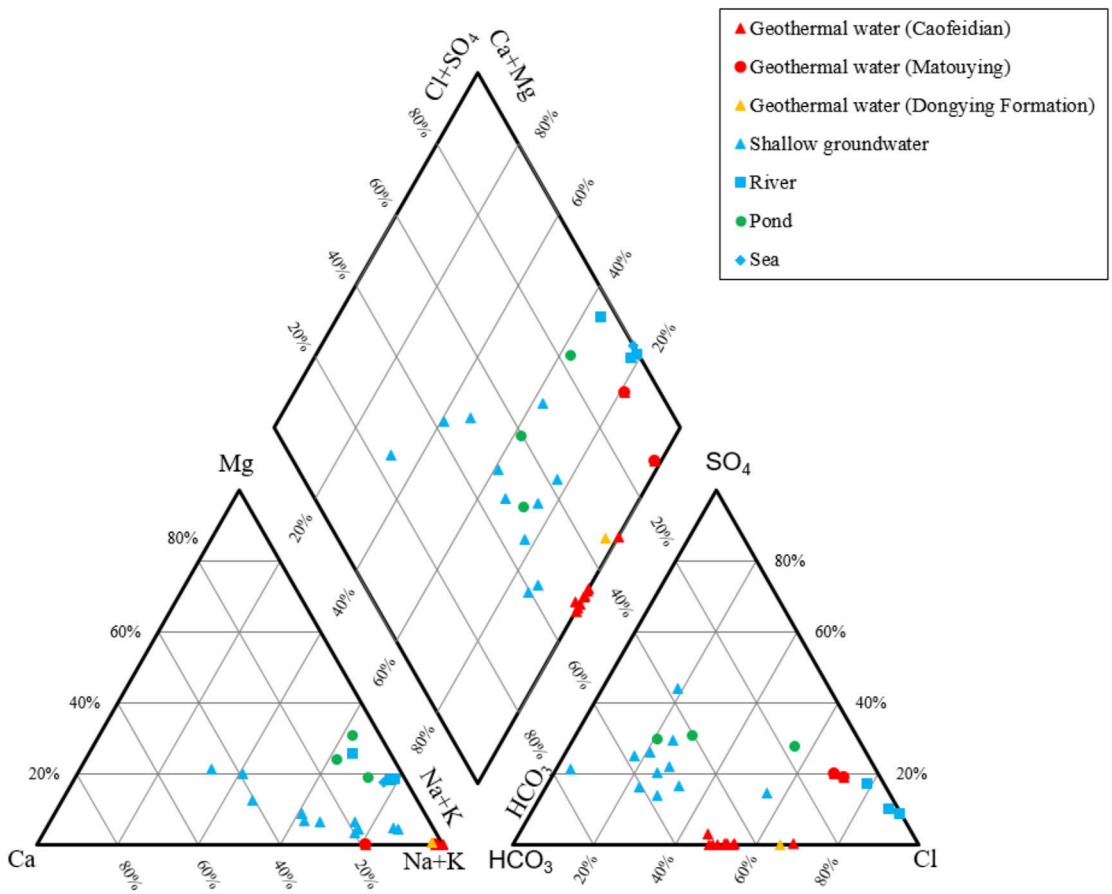

FIGURE 6 | Piper diagram of different water bodies around geothermal sites.

TABLE 1 | Chemical and isotope composition of water samples at Nanpu Sag.

Sample label	Type	Date	Depth(m)	pH	T (°C)	EC (μs/cm)	TDS (mg/L)	Na^+ (mg/L)	K^+ (mg/L)	Mg^{2+} (mg/L)	Ca^{2+}(mg/L)	F^- (mg/L)	Cl^- (mg/L)	NO_3^- (mg/L)	SO_4^{2-} (mg/L)	CO_3^{2-} (mg/L)	HCO_3^- (mg/L)	Water types	$\delta^{18}O$ (‰)	δ^2H (‰)
P-1	Pond	1-Dec-2019	—	8.23	0	1,194	531	97.4	6.27	20.73	20.13	0.84	71.81	3.01	103.84	0	174.12	HCO_3-Cl-SO_4-Na-Mg-Ca	−2.61	−31.87
P-2		1-Dec-2019	—	8.46	4.4	3,581	1789	461.36	27.37	65.4	50.69	1.75	85.44	0	166.6	0	354.51	HCO_3-SO_4-Cl-Na-Ca	−1.82	−26.79
P-3		1-Dec-2019	—	9.25	0	1,647	834	171.97	8.01	45.66	16.43	0.76	223.85	0	151.52	19.71	116.5	Cl-SO_4-HCO_3-Na-Mg-Ca	−1.93	−30.5
P-4		4-Dec-2019	—	8.56	2.6	2,900	2,600	590.27	41.44	154.85	31.52	1.67	1,053.62	0	289.28	30.8	299.39	Cl-SO_4-HCO_3-Na-Mg	1.29	-7.56
P-5		6-Dec-2019	—	9.33	3.5	2,810	2,460	828.44	27.6	77.44	22.44	1.54	1,027.26	0	86.17	67.76	388.33	Cl-HCO_3 -Na	−0.74	−23.37
R-1	River	1-Dec-2019	—	8.86	0	3,780	2,138	1,175.3	55.57	254.58	152.04	30.07	2,139.52	0	637.39	27.1	190.41	Cl-SO_4 -Na	−0.83	−18.68
R-2		4-Dec-2019	—	7.78	1.7	9,390	9,280	1,310.82	50.69	167.66	57.99	2.28	2,473.26	0	388.31	0	124.02	Cl -Na	−4.11	−37.96
R-3		6-Dec-2019	—	8.79	2.2	1,155	11,230	2,243.91	67.58	301.14	81.9	5.95	4,218.2	0	582.56	24.64	206.69	Cl -Na	−4.82	−42.52
R-4		6-Dec-2019	—	8.66	4.2	498	399	42.05	5.23	24.12	60.52	0.55	53.91	11.99	121.66	2.46	120.26	HCO_3-SO_4-Cl -Na-Ca-Mg	−7.4	−55.8
S-1	Sea	4-Dec-2019	—	8.05	2.6	2,770	2,910	9,186.84	374.69	1,149.19	609.47	5.2	18,249.49	0	2,386.67	0	97.71	Cl -Na	−0.96	−9.65
S-2		4-Dec-2019	—	7.93	2.8	2,530	2,610	8,720.65	349.9	1,112.36	244.37	9.98	16,804.85	0	2,237.45	0	102.72	Cl -Na	−1.41	−12.93
WL-1	Shallow groundwater	30-Nov-2019	200	8.2	28	561	280	83.75	1.07	2.52	17.67	0.78	29.88	0	32.15	11.09	108.98	HCO_3-Na-Ca	−10.08	−76.02
WL-2		1-Dec-2019	300–400	8.19	14	652	327	74.39	0.59	3.31	15.98	0.86	33.5	0	53.84	12.32	106.48	HCO_3-SO_4-Cl-Na-Ca	−10.19	−77.07
WL-3		1-Dec-2019	200	7.9	13.5	608	305	37.99	0.45	9.96	32.05	0.51	22.17	0	43.55	0	126.52	HCO_3-SO_4-Cl-Na-Ca	−9.73	−74.89
WL-4		1-Dec-2019	470	8.27	9	593	294	82.93	0.83	1.98	18.7	1.07	27.34	8.23	87.57	0	95.2	Cl-HCO_3-SO_4-Na-Ca	−9.97	−76.44
WL-5		2-Dec-2019	100	7.67	—	568	300	115.2	1.08	3.12	10.18	0.81	38.9	0.77	25.78	0	134.04	HCO_3-Na	−10.02	−75.34
WL-6		4-Dec-2019	280	7.9	13.3	441	273	69.01	0	5.22	29.84	0.28	43.62	0.59	29.92	0	116.5	HCO_3-Cl-SO_4-Na-Ca	−9.96	−77.44
WL-7		4-Dec-2019	300	8.33	16.8	470	283	101.53	0.7	2.96	10.21	0.93	28.94	0.25	27.79	4.93	131.53	HCO_3-Cl-SO_4 -Na	−10	−74.61
WL-8		6-Dec-2019	230	7.8	15.3	393	237	72.61	0.73	3.66	25.83	0.3	22.99	0	39.37	0	101.47	HCO_3-Cl-SO_4-Na-Ca	−10.2	−75.97
WL-9		6-Dec-2019	280	8	16	705	437	104.27	0.92	5.85	44.87	0.52	120.66	0	42.83	0	113.99	Cl-HCO_3-SO_4 -Na-Ca	−10.07	−74.97
WL-10		6-Dec-2019	230	7.97	13.6	475	303	64.02	0.76	8.97	48.62	0.23	42.07	0	45.29	0	131.53	HCO_3-Cl-SO_4 - Na-Ca	-9.67	-76.11
WL-11		6-Dec-2019	230	7.84	13.5	369	233	36.35	0.46	12.58	45.43	0.26	3.77	0	31.23	0	140.3	HCO_3-SO_4-Cl -Na-Ca	-9.85	-71.45
WR-1	Geothermal water (Caofeidian)	28-Nov-2019	2,422	8.2	77.7	1,635	833	229.29	3.38	0	0	6.03	145.8	0	0.81	33.26	207.94	Cl-HCO_3-Na	−9.23	−73.19
WR-2		29-Nov-2019	2,332	8.37	79.4	1,484	733	231.95	3.83	0	0	5.17	140.42	0	0.42	19.71	107.73	Cl-HCO_3-Na	−9.44	−73.51
WR-3		29-Nov-2019	2,497	8.49	77.4	1,379	691	220.62	3.18	0	0	5.8	135.34	0	0	11.09	229.24	Cl-HCO_3-Na	−9.27	−72.79
WR-4		29-Nov-2019	2,388	8.46	78.2	1,390	703	219.13	3.45	0	0	5.69	147.05	0	1.14	7.39	226.73	Cl-HCO_3-Na	−9.35	−73.06
WR-5		29-Nov-2019	2,442	8.47	79.2	1,510	752	225.36	3.65	0	0	5.8	146.79	0	1.7	14.78	231.75	Cl-HCO_3-Na	−9.26	−73.13
WR-6		29-Nov-2019	2,476	8.42	78	1,433	704	216.34	3.15	0	0	5.52	143.42	0	0	13.55	209.2	Cl-HCO_3-Na	-9.32	-73.22
WR-7		29-Nov-2019	2,475	8.37	70	1,539	767	247.27	4.33	0	0	6.13	153.6	0	0	13.55	271.83	Cl-HCO_3-Na	−9.27	−73.01
WR-8		29-Nov-2019	2,500	8.4	76.3	1,524	762	235.8	3.49	0	3.09	6.35	136.86	0	12.42	13.55	255.55	Cl-HCO_3-Na	−9.28	−76.11
WR-9		29-Nov-2019	2,534	8.43	80	1,475	740	233.51	3.7	0	0	5.89	150.25	0	0	17.25	234.25	Cl-HCO_3-Na	−9.27	−73.2
WR-10		30-Nov-2019	—	8.42	81	1,673	831	279.5	4.72	0	0	6.36	162	1.84	0.47	12.32	296.88	Cl-HCO_3-Na	−9.18	−72.83
WR-11	Geothermal water (Matouying)	30-Nov-2019	—	8.52	117	2,794	1,408	346.33	13.63	0	71.24	16.04	433	0	155.19	11.09	91.45	Cl-SO_4-HCO_3-Na	−8.18	−70.73
WR-12		30-Nov-2019	—	7.27	—	2,239	1,111	306.67	7.26	0	4.41	12.21	370.99	0	144.38	0	100.21	Cl-SO_4-HCO_3-Na	−8.28	−71.37
D-1	Geothermal water (Dongying Formation)	3-Dec-2019	2,161–2,492	8.15	8	3,990	2,260	774.01	16.79	2.67	16.88	3.5	735.3	0	0	0	652.65	Cl-HCO_3-Na	−8.25	−69.31

fields was less than 20 km, a significant difference was observed in the temperature patterns at the two sites. **Figure 4** also illustrates that there are significant thermal disturbances near the Gaoliu Fault, indicating that the Gaoliu and Xinanzhuang faults are important channels for the migration of geothermal water. The rapid changes in temperature near the Baigezhuang Fault suggest the presence of a barrier dividing Caofeidian and Matouying into two geothermal systems. The Xinanzhuang, Baigezhuang, and Gaoliu faults in the study area are the main heat-controlling and water-controlling structures. From the contour of hydrostatic pressure of geothermal water at the depth of 2000m (**Figure 5**), it can be concluded that the flow direction of geothermal water is from northwest to southeast at Caofeidian, which keeps in accordance with the modeling results by Huang et al. (2021b).

Hydrochemistry Characteristic

All water samples are plotted in **Figure 6** and shown in **Table 1**. The results show that the chemical characteristics of geothermal water at Caofeidian and Matouying are distinct. For geothermal water at the Caofeidian, the TDS ranges from 691 mg/L to 833 mg/L, with an average value of approximately 750 mg/L. In addition, the water type was characterized by the presence of Cl·HCO_3-Na. The pH was between 8.2 and 8.49. The principal cation was Na^+ (219–279.0 mg/L) and the concentration of K^+ was low, ranging from 3.1 to 4.7 mg/L. Ca^{2+} and Mg^{2+} were not detected in any of the 10 geothermal boreholes. For geothermal water at the Matouying, the TDS values were 1,111 mg/L and 1,408 mg/L, which were greater than those observed at the Matouying. The principal cations were also Na^+ (306 mg/L and 346 mg/L), and the principal anions were Cl^-, SO_4^{2-}, and HCO_{3-}. The geothermal water at Matouying was Cl·SO_4·HCO_3-Na, with pH was 7.27 and 8.52.

The TDS of the shallow groundwater ranged from 233 mg/L to 437 mg/L. The pH range of the shallow groundwater was 7.67–8.33. The principal cation was Na^+(36–104 mg/L), which was found in greater concentrations than K^+ (0–1.08 mg/L), Ca^{2+}(10.2–48.6 mg/L), and Mg^{2+}(2.0–12.58 mg/L). The principal anions were Cl^-, HCO_3^-, and SO_4^{2-}. The shallow groundwater water types were HCO_3-Na·Ca and HCO_3·SO_4·Cl-Na·Ca. The TDS of surface water, including river water, pond water, and sea water, was much higher than that of groundwater.

Water Isotopic Composition

The stable isotope compositions of the water samples are shown in **Figure 7** and **Table 1**, which indicate that stable isotopes of shallow groundwater are located in relatively centralized region with a range of -9.7‰ to -10.2‰ for $\delta^{18}O$ and a range of -77.4‰ to -71.5‰ for δ^2H. We can easily distinguish between the two groups of geothermal water at the Caofeidian and the Matouying. For geothermal water at the Caofeidian, stable isotopes ranged from -9.4‰ to -9.2‰ for $\delta^{18}O$ and from -76.1‰ to –72.8‰ for δ^2H, respectively. The stable isotopes of geothermal water at Matouying are more enriched than other groundwater samples with $\delta^{18}O$ values of -8.2‰ and -8.3‰ and δ^2H values of -70.7‰ and -71.4‰, respectively. The stable isotopes of rivers, ponds, and seas are much more enriched than those of the sampled groundwater. In addition, the local meteoric line (LMWL) presented in previous studies by Fang et al. (2014), and the equation is $\delta^2H = 6.61\delta^{18}O+0.69$. We found that shallow groundwater was distributed along the LMWL, whereas the sampling geothermal waters were all located below the LMWL.

Groundwater Dating

Based on the hypothesis that dissolved inorganic carbon (DIC) is derived from soil CO_2 and carbonate dissolution, the $\delta^{13}C$ mixing model was used to calculate and correct the groundwater ^{14}C age based on the significant difference in $\delta^{13}C$ values between soil CO_2 and carbonate minerals (Huang and Pang, 2011; Kong et al., 2020). The groundwater ages of the geothermal water samples are shown in **Table 2**.

As can be seen from **Table 2**, the geothermal water ^{14}C at Caofeidian is 1.01–1.98 PMC, and the estimated age is 27-32 ka. The geothermal water ^{14}C at Matouying is 3.16 PMC, and the estimated age is about 21 ka. In general, the geothermal water at Matouying formed more recently than that of the Caofeidian, which indicates a different circulation pattern at the two sites.

DISCUSSION

Recharge Source of Geothermal Water

Comparing the hydrochemical composition of geothermal water with shallow groundwater, the water types were different, and the concentrations of K^+ and Cl^- were significantly greater in geothermal water (**Figure 6** and **Table 1**). The greater TDS value of geothermal water indicates the geological process by which precipitation infiltrates into the ground and then interacts with the minerals through which it flows (Domenico and Schwartz, 1998; Ma et al., 2011). The isotope composition of geothermal water at both sites deviated from the LMWL and was more enriched in ^2H and ^{18}O than in shallow groundwater (**Figure 7**). For the isotope enrichment of geothermal water, we propose some hypothesis to address the $\delta^{18}O$-δ^2H pattern of geothermal water in **Figure 7**, including evaporation process, water-rock interaction, mixing process and bacterial SO_4^{2-} reduction process (BSR). First, the evaporation process is usually expressed by evaporation line of surface water like ponds and lakes within a study area. However, the geothermal water isotopes is located far below the water line of ponds water isotope (**Figure 7**), which could provide robust evidence to exclude the hypothesis of evaporation. Considering the different isotopic signature of geothermal water, geological settings and hydrothermal patterns at Caofeidian and Matouying, the $\delta^{18}O$-δ^2H pattern as well as the recharge source of geothermal water at the two places are investigated respectively. For the geothermal water at Caofeidian, the ^{18}O enrichment of geothermal water may be due to the water-rock interaction with surrounding minerals at certain pressures and temperatures (Pang et al., 2017). For the ^2H enrichment of geothermal water at Caofeidian, we attribute it to the process of bacterial SO_4^{2-} reduction (BSR), which converts SO_4^{2-} to H_2S and accompanies the enrichment for ^2H. The low concentration of SO_4^{2-} in geothermal water provides evidence for the occurrence of the BSR process (Matray et al., 1994). Such phenomenon has also been detected in the geothermal water of Niutuizhen reservoir, northern China (Kong et al., 2020). However, the reduction of

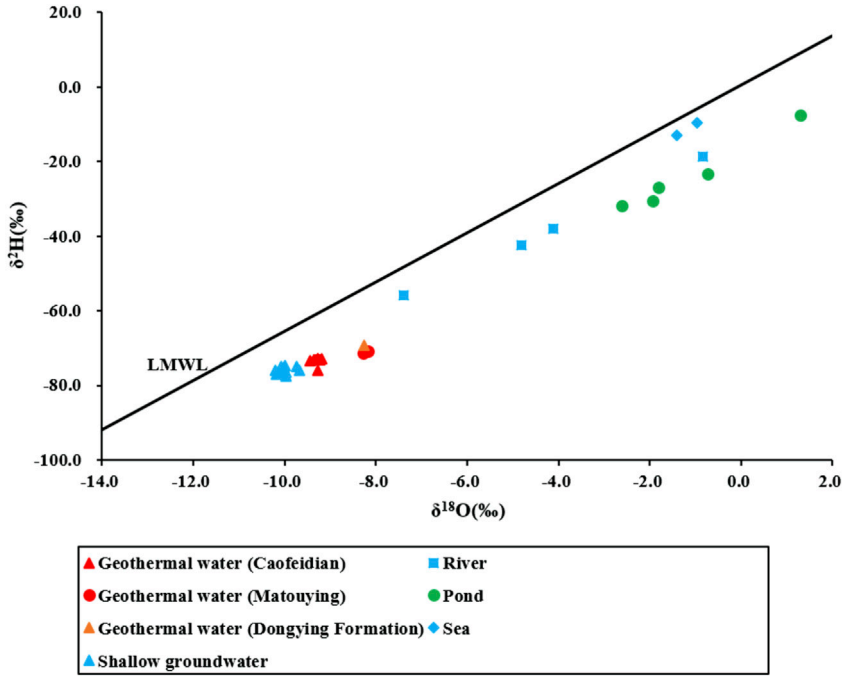

FIGURE 7 | Isotopes of all the water samples at the Caofeidian and the Matouying.

TABLE 2 | Groundwater age of geothermal water at the Caofeidian and the Matouying.

Sample Label	Region	^{14}C (pmc)	$\delta^{13}C$ (‰)	Age
WR-8	Caofeidian	1.01	−11.5	32,258
WR-9	Caofeidian	1.98	−11.7	26,836
WR-11	Matouying	3.16	−9.1	20,894

SO_4^{2-} (approximately 0.05 g) was not sufficient to increase ^2H by 0.5‰. There are other reasons for the enrichment of ^2H. We attribute this to the mixing process with groundwater from the underlying Dongying Formation, which may recharge the upper Guantao Formation with more enriched isotopes through the faults connecting the two formations (**Figure 3**). As for the Matouying geothermal water, the even more enriched isotopes can be attributed to the water-rock interaction under higher temperature conditions. The high value of $^{87}Sr/^{86}Sr$ for geothermal water at the Matouying also suggests that the geothermal water has experienced deep circulation into the granite strata at higher temperatures (Barbieri & Morotti, 2003; Guo et al., 2009; Khaska et al., 2015). Besides, the much higher concentration of Li and B of geothermal water than that in the shallow groundwater can also be a good indicator for the deep circulation of geothermal water (Giggenbach et al., 1995).

Reservoir Temperature Calculation

Considering the low concentrations of Ca^{2+} and Mg^{2+} in the geothermal water in the study area, Na-K geothermometers were employed for the calculation of the reservoir temperature (Fournier, 1979; Arnorsson et al., 1983; Pang & Reed, 1998). According to the calculation results of the Na-K geothermometers, the estimated reservoir temperature is completely different between the geothermal water at Caofeidian and Matouying (**Table 3**). The reservoir temperature at the Caofeidian is 83–92°C while the reservoir temperature at the Matouying is 107–137°C, which also indicates the different geothermal systems at the two sites.

Heat Sources

The reservoir temperature of the geothermal water at the Matouying is much greater than that at Caofeidian (**Table 2**). We attribute the thermal anomalies at the Matouyong to the normal thermal conductivity as well as the radioactive heat generated by the granite (Wang, 2015b; Zhang et al., 2020a). The much greater concentration of radioactive heat-generating elements including uranium (U), thorium (Th), and potassium (K) observed in geothermal water at the Matouying suggests the existence of additional radioactive heat (**Table 4**). In addition, the higher concentration of Sr and $^{87}Sr/^{86}Sr$ of geothermal water at Matouying transports the signal from potassium-rich rocks, which also indicates the additional radioactive heat generated from granite (Faure & Powell, 2012; Capo et al., 1998). And the radioactive heat from granite has also been illustrated in the granite of the Bohai Bay Basin (Jiang et al., 2016; Li et al., 2017; Qiu et al., 2015). Thus, it can be concluded that part of the heat source of the geothermal water at Matouying originates from the heat generated by granite radioactive elements, which is different from the heat source of the geothermal water at the Caofeidian, which originates from the natural geothermal heating of the earth's crust.

TABLE 3 | Estimated reservoir temperature at the Caofeidian and the Matouying.

Sampling Lable	WR-1	WR-2	WR-3	WR-4	WR-5	WR-6	WR-7	WR-8	WR-9	WR-10	WR-11	WR-12
	Caofeidian										Matouying	
T (°C)	83.6	89.7	82.6	86.8	88.1	83.1	92	83.9	87.1	90.2	136.6	107.4

TABLE 4 | Trace elements (Li, B, U, Th, Sr) and $^{87}Sr/^{86}Sr$ characteristic of geothermal water at the Caofeidian and the Matouying.

Sample lable	Type	Li (μg/L)	B (μg/L)	Sr (μg/L)	U (μg/L)	Th (μg/L)	$^{87}Sr/^{86}Sr$
WL-1	Shallow groundwater	9.53	6	401	0.044	<0.002	0.708,895
WL-3		6.69	<0.002	870	0.045	<0.002	0.709,043
WL-6		6.41	1	674	0.036	<0.002	0.70894
WL-9		5.4	<0.002	845	0.048	<0.002	0.708,938
WL-11		4.9	3	764	0.05	<0.002	0.709,244
WR-1	Caofeidian geothermal water	38.4	311	69.6	0.002	0.02	0.708,236
WR-8		35.9	284	92.8	0.003	0.005	0.70998
WR-9		31.2	343	106	<0.002	0.003	0.708,136
WR-11	Matouying geothermal water	657	739	591	0.012	0.008	0.718,459

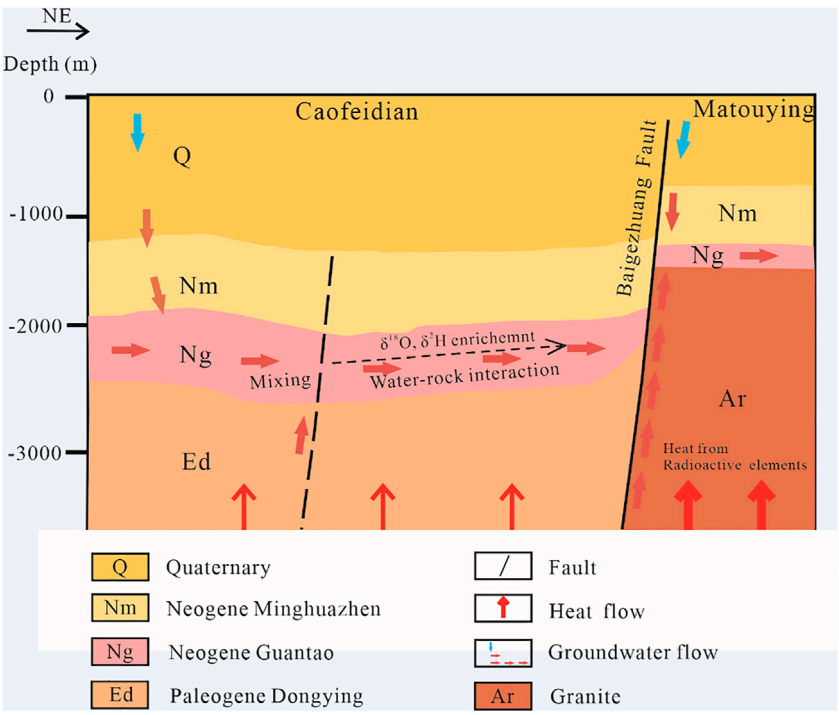

FIGURE 8 | Conceptual model of hydrothermal genesis of the Caofeidian and the Matouying geothermal reservoirs.

Conceptual Genetic Model

Based on the above analysis with regard to the geological setting, hydrothermal pattern, geochemical, and isotopic data, a conceptual genetic model of the geothermal water in our study area is proposed in **Figure 8**. Generally, all geothermal water originates from local precipitation. Then, the different infiltrated water flow pathways would result in distinct geothermal water at the two observation sites. The geothermal water rises upward through deep faults and fractures, which can be regarded as hydrothermal channels. Quaternary deposits comprising immature yellow gravel and clay interbeds serve as cap rocks for geothermal systems. The

geochemical and isotopic composition of geothermal water at the Caofeidian indicate that the infiltrated water would experience the water-rock reaction with the sandstone along its pathways, the BSR process, and the mixing process from deeper Ed geothermal water. The Geothermal water flow direction is from the northwest to the southeast. The geothermal water heating source at the Caofeidian is thermal conductivity and fluid convection. The Baigezhuang fault functions as a barrier to divide the two geothermal systems. Geothermal water at the Matouying would infiltrate deep into the granite and ascend at higher temperatures. Thus, the heat generated from radioactive elements within the granite is an additional heat source for geothermal water in the Matouying.

CONCLUSION

We found different hydrothermal patterns at the Caofeidian and the Matouying geothermal systems through water temperature and pressure monitoring. By conducting detailed geochemical and isotopic analyses of the geothermal water, we investigated the hydrothermal system characteristics of the two geothermal systems and distinguished the recharge source and circulation pattern of geothermal water at the two sites. Although geothermal water originates from precipitation at both systems, the circulation pattern of groundwater is distinct for tthem. The geothermal water at Caofeidian has experienced the process of infiltration, interaction with sandstone, BSR, and mixing with geothermal water from the underlying Dongying Formation. The infiltrated water is able to circulate deeply into the granite underlying the Matouying system. Application of Na-K geothermometers indicated reservoir temperatures to be in the interval of 83–92°C at the Caofeidian and 107–137°C at the Matouying, respectively. The corrected ^{14}C age of geothermal water indicates a lower circulation rate and rare renewability for geothermal water at the Caofeidian system. This study provides multiple information on the geothermal systems in our study area, and the results are instructive and significant with respect to the sustainable exploitation of geothermal resources in the Caofeidian and the Matouying geothermal systems.

DATA AVAILABILITY STATEMENT

The original contributions presented in the study are included in the article/Supplementary Material, further inquiries can be directed to the corresponding authors.

AUTHOR CONTRIBUTIONS

YK and WS designed the study and gave conceptual advice. KW, CH, and SP conducted field work, analyzed the laboratory results, and prepared the manuscript. LR, JW, and YD provided row data information and basic information about the geothermal wells. YC, YH, and FT contributed to the geological settings section. DQ, WZ, and FM conducted laboratory analysis of the samples. All authors contributed to the editing of the manuscript, and approval of the content in its current form.

FUNDING

This work was financially supported by the National Key Research and Development Program of China (Grant no. 2019YFB1504101). We also acknowledge the financial support from National Natural Science Foundation of China (Grant no. 52192623), the Youth Innovation Promotion Association of Chinese Academy of Sciences (Grant no. 2020067) and the PetroChina Jidong Oilfield Company.

ACKNOWLEDGMENTS

We thank the PetroChina Jidong Oilfield Company for providing the data used in this work and the staff like Liping Yuan, Chaoqun Liu and other individuals who helped the field sampling work.

REFERENCES

An, Q., Wang, Y., Zhao, J., Luo, C., and Wang, Y. (2016). Direct Utilization Status and Power Generation Potential of Low-Medium Temperature Hydrothermal Geothermal Resources in Tianjin, China: A Review. *Geothermics* 64, 426–438. doi:10.1016/j.geothermics.2016.06.005

Arnórsson, S., Gunnlaugsson, E., and Svavarsson, H. (1983). The Chemistry of Geothermal Waters in Iceland. III. Chemical Geothermometry in Geothermal Investigations. *Geochimica et Cosmochimica Acta*, 47(3), 567–577. doi:10.1016/0016-7037(83)90278-8

Barbieri, M., and Morotti, M. (2003). Hydrogeochemistry and Strontium Isotopes of spring and mineral Waters from Monte Vulture Volcano, Italy. *Appl. Geochem.* 18 (1), 117–125. doi:10.1016/S0883-2927(02)00069-0

Byrappa, K., and Yoshimura, M. (2012). *Handbook of Hydrothermal Technology*. New York: William Andrew.

Capo, R. C., Stewart, B. W., and Chadwick, O. A. (1998). Strontium Isotopes as Tracers of Ecosystem Processes: Theory and Methods. *Geoderma*, 82(1-3), 197–225. doi:10.1016/S0016-7061(97)00102-X

Chang, J., Qiu, N. S., Zhao, X. Z., Xu, W., Xu, Q. C., Jin, F. M., et al. (2016). Present-day Geothermal Regime of the Jizhong Depression in Bohai Bay basin, East China. *Chin. J. Geophysics-Chinese Edition* 59 (3), 1003–1016. doi:10.6038/cjg20160322

Clark, I. D., and Fritz, P. (2013). *Environmental Isotopes in Hydrogeology*. Boca Raton: CRC Press. doi:10.1201/9781482242911

Domenico, P. A., and Schwartz, F. W. (1998). *Physical and Chemical Hydrogeology*. New York: Wiley, (Vol. 506).

Dong, Y., Wang, Z., Zheng, H., and Xu, A. (2008). Control of Strike-Slip Faulting on Reservoir Formation of Oil and Gas in Nanpu Sag. *Pet. Exploration Dev.* 35 (4), 424–430. doi:10.1016/s1876-3804(08)60090-7

Dong, Y., Huang, H., Ren, L., Li, H., Du, Z., E, J., et al. (2021). Geology and Development of Geothermal Field in Neogene Guantao Formation in Northern Bohai Bay Basin: A Case of the Caofeidian Geothermal Heating Project in Tangshan, China. *Pet. Exploration Dev.* 48 (3), 775–786. doi:10.1016/S1876-3804(21)60063-0

Duan, Z., Pang, Z., and Wang, X. (2011). Sustainability Evaluation of limestone Geothermal Reservoirs with Extended Production Histories in Beijing and Tianjin, China. *Geothermics* 40 (2), 125–135. doi:10.1016/j.geothermics.2011.02.001

Fang, C., Liu, F. T., Meng, L. S., Liu, H. W., Qin, Y. F., and Zheng, J. N. (2014). Application of Hydrogen and Oxygen Isotopes to Study Hydrologic Cycle in the Caofeidian Area. *North. China Geology.* (2), 102–107.

Faure, G., and Powell, J. L. (2012). *Strontium Isotope Geology*, 5. Springer Science & Business Media.

Fournier, R. O. (1979). A Revised Equation for Na/K Geothermometers. *Geoth Res. Counc. Trans.* 3, 221–224. doi:10.1016/0016-7037(73)90060-4

Giggenbach, W. F., Stewart, M. K., Lyon, G. L., Sano, Y., and Goguel, R. L. (1995). *Isotopic and Chemical Composition of Waters and Gases from the East Coast Accretionary Prism*. New Zealand.

Guo, Q., Wang, Y., and Liu, W. (2009). O, H, and Sr Isotope Evidences of Mixing Processes in Two Geothermal Fluid Reservoirs at Yangbajing, Tibet, China. *Environ. Earth Sci.* 59 (7), 1589–1597. doi:10.1007/s12665-009-0145-y

Hähnlein, S., Bayer, P., Ferguson, G., and Blum, P. (2013). Sustainability and Policy for the thermal Use of Shallow Geothermal Energy. *Energy Policy* 59, 914–925. doi:10.1016/j.enpol.2013.04.040

Huang, T., and Pang, Z. (2011). "*Combined Conceptual Model (V& P Model) to Correct* Groundwater Radiocarbon Age," in Paper presented at the 2011 International Symposium on Water Resource and Environmental Protection, 20–22.

Huang, Y., Pang, Z., Kong, Y., and Watanabe, N. (2021a). Assessment of the High-Temperature Aquifer Thermal Energy Storage (HT-ATES) Potential in Naturally Fractured Geothermal Reservoirs With a Stochastic Discrete Fracture Network Model. *J. Hydrol.* 603, 127188. doi:10.1016/j.jhydrol.2021.127188

Huang, Y., Cheng, Y., Ren, L., Tian, F., Pan, S., Wang, K., et al. (2021b). Assess the Geothermal Resource Potential of an Active Oil Field by Integrating a 3D Geological Model with the Hydro-thermal Coupled Simulation. *Front. Earth Sci.* 1178. doi:10.3389/feart.2021.787057

Jiang, G., Gao, P., Rao, S., Zhang, L., Tang, X., Huang, F., et al. (2016). Compilation of Heat Flow Data in the Continental Area of China. *Chin. J. Geophys.* 59 (8), 2892–2910.

Khaska, M., Le Gal La Salle, C., Videau, G., Flinois, J.-S., Frape, S., Team, A., et al. (2015). Deep Water Circulation at the Northern Pyrenean Thrust: Implication of High Temperature Water-Rock Interaction Process on the Mineralization of Major spring Water in an Overthrust Area. *Chem. Geology.* 419, 114–131. doi:10.1016/j.chemgeo.2015.10.028

Kong, Y., Pang, Z., Pang, J., Li, J., Lyu, M., and Pan, S. (2020). Fault-Affected Fluid Circulation Revealed by Hydrochemistry and Isotopes in a Large-Scale Utilized Geothermal Reservoir. *Geofluids* 2020, 1–13. doi:10.1155/2020/2604025

Kong, Y., Pang, Z., Shao, H., Hu, S., and Kolditz, O. (2014). Recent Studies on Hydrothermal Systems in China: a Review. *Geothermal Energy* 2 (19). doi:10.1186/s40517-014-0019-8

Le Gal, V., Lucazeau, F., Cannat, M., Poort, J., Monnin, C., Battani, A., et al. (2018). Heat Flow, Morphology, Pore Fluids and Hydrothermal Circulation in a Typical Mid-Atlantic Ridge Flank Near Oceanographer Fracture Zone. *Earth Planet. Sci. Lett.* 482, 423–433. doi:10.1016/j.epsl.2017.11.035

Li, Z., Zuo, Y., Qiu, N., and Gao, J. (2017). Meso-Cenozoic Lithospheric thermal Structure in the Bohai Bay Basin, Eastern North China Craton. *Geosci. Front.* 8 (5), 977–987. doi:10.1016/j.gsf.2016.09.003

Lister, C. R. B. (1980). Heat Flow and Hydrothermal Circulation. *Annu. Rev. Earth Planet. Sci.*, 8, 95–117. doi:10.1146/annurev.ea.08.050180.000523

Lund, J. W., and Toth, A. N. (2021). Direct Utilization of Geothermal Energy 2020 Worldwide Review. *Geothermics* 90, 101915. doi:10.1016/j.geothermics.2020.101915

Ma, R., Wang, Y., Sun, Z., Zheng, C., Ma, T., and Prommer, H. (2011). Geochemical Evolution of Groundwater in Carbonate Aquifers in Taiyuan, Northern China. *Appl. Geochem.* 26 (5), 884–897. doi:10.1016/j.apgeochem.2011.02.008

Marrasso, E., Roselli, C., Sasso, M., and Tariello, F. (2018). Global and Local Environmental and Energy Advantages of a Geothermal Heat Pump Interacting with a Low Temperature thermal Micro Grid. *Energ. Convers. Manag.* 172, 540–553. doi:10.1016/j.enconman.2018.07.028

Matray, J. M., Lambert, M., and Fontes, J. C. (1994). Stable Isotope Conservation and Origin of saline Waters from the Middle Jurassic Aquifer of the Paris Basin, France. *Appl. Geochem.*, 9(3), 297–309. doi:10.1016/0883-2927(94)90040-X

Moya, D., Aldás, C., and Kaparaju, P. (2018). Geothermal Energy: Power Plant Technology and Direct Heat Applications. *Renew. Sust. Energ. Rev.* 94, 889–901. doi:10.1016/j.rser.2018.06.047

Pang, Z.-H., and Reed, M. (1998). Theoretical Chemical Thermometry on Geothermal Waters: Problems and Methods. *Geochimica et Cosmochimica Acta*, 62(6), 1083–1091. doi:10.1016/S0016-7037(98)00037-4

Pang, Z., Kong, Y., Li, J., and Tian, J. (2017). An Isotopic Geoindicator in the Hydrological Cycle. *Proced. Earth Planet. Sci.* 1517, 534–537. doi:10.1016/j.proeps.2016.12.135

Pang, Z., Kong, Y., Shao, H., and Kolditz, O. (2018). Progress and Perspectives of Geothermal Energy Studies in China: from Shallow to Deep Systems. *Environ. Earth Sci.* 77 (16). doi:10.1007/s12665-018-7757-z

Qiu, N., Xu, W., Zuo, Y., and Chang, J. (2015). Meso-Cenozoic thermal Regime in the Bohai Bay Basin, Eastern North China Craton. *Int. Geology. Rev.* 57 (3), 271–289. doi:10.1080/00206814.2014.1002818

Qiu, N., Zuo, Y., Chang, J., and Li, W. (2014). Geothermal Evidence of Meso-Cenozoic Lithosphere Thinning in the Jiyang sub-basin, Bohai Bay Basin, Eastern North China Craton. *Gondwana Res.* 26 (3-4), 1079–1092. doi:10.1016/j.gr.2013.08.011

Qiu, N., Zuo, Y., Xu, W., Li, W., Chang, J., and Zhu, C. (2016). Meso-Cenozoic Lithosphere Thinning in the Eastern North China Craton: Evidence from thermal History of the Bohai Bay Basin, North China. *J. Geology.* 124 (2), 195–219. doi:10.1086/684830

Rybach, L. (2003). Geothermal Energy: Sustainability and the Environment. *Geothermics* 32 (4-6), 463–470. doi:10.1016/S0375-6505(03)00057-9

Shortall, R., Davidsdottir, B., and Axelsson, G. (2015). Geothermal Energy for Sustainable Development: A Review of Sustainability Impacts and Assessment Frameworks. *Renew. Sust. Energ. Rev.* 44, 391–406. doi:10.1016/j.rser.2014.12.020

Wang, E., Feng, Y., Liu, G., Chen, S., Wu, Z., and Li, C. (2021). Hydrocarbon Source Potential Evaluation Insight into Source Rocks-A Case Study of the First Member of the Paleogene Shahejie Formation, Nanpu Sag, NE China. *Energ. Rep.* 7, 32–42. doi:10.1016/j.egyr.2020.11.099

Wang, E., Li, C., Feng, Y., Song, Y., Guo, T., Li, M., et al. (2022). Novel Method for Determining the Oil Moveable Threshold and an Innovative Model for Evaluating the Oil Content in Shales. *Energy* 239, 121848. doi:10.1016/j.energy.2021.121848

Wang, E., Liu, G., Pang, X., Li, C., Zhao, Z., Feng, Y., et al. (2020). An Improved Hydrocarbon Generation Potential Method for Quantifying Hydrocarbon Generation and Expulsion Characteristics with Application Example of Paleogene Shahejie Formation, Nanpu Sag, Bohai Bay Basin. *Mar. Pet. Geology.* 112, 104106. doi:10.1016/j.marpetgeo.2019.104106

Wang, G.-l., Zhang, W., Zhang, W., Ma, F., Lin, W.-j., Liang, J.-y., et al. (2018). Overview on Hydrothermal and Hot Dry Rock Researches in China. *China Geology.* 1 (2), 273–285. doi:10.31035/cg2018021

Wang, J. (2009). "Discussions on Geothermal Energy Exploration and Utilization of China, from the point of World Geothermal Energy," in Proceedings of workshop on Chinese scientific geothermal energy exploration (Beijing: Geology Press).

Wang, J. (2015a). Geothermal Energy Should Play a More Important Role in the Smog Control and Space Heating/Refrigeration in China. *Scientific Tech. Rev.* 33 (24), 1.

Wang, J. (2015b). *Geothermics and its Application*. Beijing: Science press.

Wang, Z. T., Rao, S., Xiao, H. P., Wang, Y. B., Jiang, G. Z., Hu, S. B., et al. (2021). Terrestrial Heat Flow of Jizhong Depression, China, Western Bohai Bay basin and its Influencing Factors. *Geothermics* 96. doi:10.1016/j.geothermics.2021.102210

Yang, P., Cheng, Q., Xie, S., Wang, J., Chang, L., Yu, Q., et al. (2017). Hydrogeochemistry and Geothermometry of Deep thermal Water in the Carbonate Formation in the Main Urban Area of Chongqing, China. *J. Hydrol.* 549, 50–61. doi:10.1016/j.jhydrol.2017.03.054

Zhang, B., Li, Y., Gao, J., Wang, G., Li, J., Xing, Y., et al. (2020a). Genesis and Indicative Significance of Hot Dry Rock in Matouying, Hebei Province. *Acta Geologica Sinica* 94 (7), 2036–2051.

Zhang, C., Hu, S., Song, R., Zuo, Y., Jiang, G., Lei, Y., et al. (2020b). Genesis of the Hot Dry Rock Geothermal Resources in the Gonghe basin: Constraints from the Radiogenic Heat Production Rate of Rocks. *Chin. J. Geophys.* 63 (7), 2697–2709.

Zhu, G., Wang, Z., and Cao, Z. (2014). Origin and Source of the Cenozoic Gas in the Beach Area of the Nanpu Sag, Bohai Bay Basin, China. *Energy Exploration & Exploitation*, 32(1), 93–111. doi:10.1260/0144-5987.32.1.93

Conflict of Interest: Authors LR and JW are employed by Jidong Oilfield Company of PetroChina. Author YD is employed by Advisory Center, China National Petroleum Corporation.

The remaining authors declare that the research was conducted in the absence of any commercial or financial relationships that could be construed as a potential conflict of interest.

Publisher's Note: All claims expressed in this article are solely those of the authors and do not necessarily represent those of their affiliated organizations, or those of the publisher, the editors and the reviewers. Any product that may be evaluated in this article, or claim that may be made by its manufacturer, is not guaranteed or endorsed by the publisher.